Self-consistent cluster calculation of binding energy and potential for positive muons in copper and copper-impurity systems

Changxin Guo* and D. E. Ellis
Department of Physics, Northwestern University, Evanston, Illinois 60201
(Received 20 August 1984)

The binding energy, potential profile, and electronic structure for positive muons in copper are calculated with the use of a molecular-cluster model in the framework of the self-consistent local-density theory. Spin polarization was considered in calculations on finite clusters including Cu_{14} and an interstitial positive muon. Different positions of the muon along the body diagonal [111], and slightly displaced from the diagonal, covering the path between octahedral O to tetrahedral T sites were considered. Both the binding energy $\Delta E_{\rm tot}(\mathbf{r})$ and the muon potential $V^{\mu}(\mathbf{r})$ exhibit a double minimum, with the O site more stable. The effects of Cu vacancies and Ni impurities on the muon in copper are considered also. Binding-energy curves show the attraction of the Cu vacancy and Ni impurity for the muon. Valence-charge-density distribution profiles for different positions of a muon along the [111] direction in μ-Cu_{14}, μ-Cu_{13}, and μ-Ni-Cu_{13} clusters are calculated.

I. INTRODUCTION

The electronic structure and associated properties of impurities in metals, in particular for light impurities, such as hydrogen and muons, is an extensive problem which has become a topic of great current interest. Some important technical applications, such as magnetic, superconducting, and mechanical properties have a direct relation to the impurity-induced properties. The muon-spin rotation (μSR) technique has been used for over ten years to study the diffusion of the muon in metals and alloys, and also emerged as a powerful probe to study spin densities, crystallographic position, etc.[1-5] The physics of muons, i.e., muon diffusion and trapping in solids and the quantum behavior of a light atom, is one more important topic in this area.

A series of experiments has been made for measuring the positive muon (μ^+) linewidth in "pure" and doped copper samples.[2,6-11] They analyzed these results within the framework of the quantum theory of diffusion and concluded the following.

(1) In pure copper, μ^+ is at an octahedral site in the 0.1—80 K temperature region. The fit of the experimental results and theoretical curves of linewidth for octahedral site assignment is good for 2, 20, and 80 K; however, the 0.1-K data do not fit the octahedral assignment as well. The tendency is nevertheless in favor of that site.

(2) In copper doped with nickel, the results indicate positive muon trapping in nonperfect regions caused by the Ni impurities.

Clawson *et al.*[3] have also done experiments to explain the phenomena of low-temperature mobility of positive muons in copper. In order to explain why the mobility of position muons in Cu increases when the temperature decreases from 5 to 0.7 K, Seeger[4] proposed a model assuming that in the case of Cu, the stable sites are octahedral interstices. The tetrahedral sites are assumed to be metastable, with a thermally activated (phonon-assisted tunneling) transition to the octahedral sites beginning at 0.7 K. Instead, Clawson suggested that the μ^+ site does not vary with temperature between 0.7 and 5 K, but that a diffusion process occurs which is limited by static disorder below 0.7 K and by thermal disorder above 5 K.

In brief, microscopic-theoretical predictions require detailed knowledge of the surrounding electronic structure and potential of the muon in the host lattice. Since a proton or a lighter muon with no core electronic structure is the simplest kind of impurity that can be implanted into a solid, the electronic structure associated with these particles in metals is perhaps also simple. A number of theoretical models have been developed,[12] such as different kinds of jellium models and molecular-cluster and band-structure calculations, to treat this case. The Hartree-Fock-Slater theory has been developed to calculate the binding energy, hyperfine fields, and electronic structure of small particles in transition metals,[13,14] and this theory represents a feasible first-principles approach.

In this paper, we use the molecular-cluster model in the framework of the Hartree-Fock-Slater self-consistent one-electron local-density theory to calculate the electronic structure, binding energies, and potential for positive muons in copper. Spin polarization was included in the calculations of finite clusters consisting of Cu_{14} and an interstitial positive muon. In order to get the binding energies of the cluster and potential profiles seen by the muon, we chose several different positions of the muon along the body-diagonal direction [111] and slightly displaced from the diagonal, covering the path including octahedral O to tetrahedral T sites in the fcc structure. For every μ^+ position, we made a separate self-consistent field (SCF) calculation. Similar calculations were done for the Cu-vacancy and Ni-impurity systems. In these cases, a cubic-corner copper atom was changed to a Cu vacancy or an Ni impurity.

II. THEORETICAL MODEL AND COMPUTATIONAL PROCEDURE

The theoretical basis for the electronic-structure calculations used here is the self-consistent one-electron local-density formalism in the Hartree-Fock-Slater (HFS) model.[15–20] The essential point of this theory is the replacement of the nonlocal Hartree-Fock exchange operator by a potential depending only on the local electron density.

In a nonrelativistic approach the one-electron Hamiltonian for the molecule can be written (in Hartree atomic units) as

$$H(\mathbf{r})=-\tfrac{1}{2}\nabla^2+V(\mathbf{r}) . \tag{1}$$

The first term is kinetic energy; $V(\mathbf{r})$ represents the molecular potential, which is taken to be a sum of Coulomb and exchange and correlation potentials

$$V(\mathbf{r})=V_C(\mathbf{r})+V_{\mathrm{xc}}(\mathbf{r}) . \tag{2}$$

Here the Coulomb potential $V_C(\mathbf{r})$ is the sum of nuclear and electronic contributions

$$V_C(\mathbf{r})=-\sum_\nu \frac{Z_\nu}{|\mathbf{r}-\mathbf{R}_\nu|}+\int \frac{\rho(\mathbf{r}')d\mathbf{r}'}{|\mathbf{r}-\mathbf{r}'|} , \tag{3}$$

where the first term is the electron-nuclear attraction, R_ν is the nuclear position of the νth atom, and the second term is electron-electron repulsion; $\rho(\mathbf{r}')$ is the total electronic charge density at position $\mathbf{r}'$.

For a spin-polarized approach, one must consider the spin-dependent exchange and correlation potential in some approximate form. The simplest form is the Kohn-Sham-Slater potential[21,22]

$$V_{\mathrm{xc},\sigma}(\mathbf{r})=-3\alpha[3\rho_\sigma(\mathbf{r})/4\pi]^{1/3} , \tag{4}$$

where ρ_σ is the density at point $\mathbf{r}$ of electrons with spin direction σ. Here α is a constant which is normally chosen as $\frac{2}{3}\le\alpha\le 1$; in this study we chose $\alpha=0.7$.

As in the usual linear combination of atomic-orbital—molecular-orbital (LCAO—MO) method, the molecular-orbital eigenfunctions are expanded in terms of symmetry orbitals,

$$\Psi^\eta_{i\sigma}(\mathbf{r})=\sum_j \chi^\eta_j(\mathbf{r})C^\eta_{ji\sigma} , \tag{5}$$

where $\eta=(k\lambda)$ denotes row λ of representation k of the molecular point group. The symmetry orbitals $\chi^\eta_j(\mathbf{r})$ are chosen here as linear combinations of atomic orbitals located on the different atoms in the molecule corresponding to the cluster point group symmetry, i.e.,

$$\chi^\eta_j(\mathbf{r})=\sum_{\nu,m} W^{jl}_{\nu m}U_{nl}(r_\nu)Y_{lm}(\hat{r}_\nu) , \tag{6}$$

where $U_{nl}(r_\nu)$ is the atomic radial wave function centered on the νth nucleus, with principal quantum number n and orbital quantum number l. U_{nl} is obtained numerically by solving a self-consistent free-atom or ion problem, and Y_{lm} is a spherical harmonic function with magnetic quantum number m. $W^{jl}_{\nu m}$ are symmetrization coefficients which can be obtained by group-theoretical projection operators.

In formula (5) the expansion coefficients (variational coefficients $C^\eta_{ji\sigma}$) are obtained using standard procedures by solving the matrix secular equation

$$(H-\epsilon S)C=0 , \tag{7}$$

where ϵ is the eigenvalue.

The Hamiltonian matrix H and the symmetry orbital overlap matrix S are obtained in the discrete variational method (DVM) as a weighted sum over a set of sample points,[23,24]

$$H_{ij}=\sum_\kappa W(\mathbf{r}_k)\chi^{*\eta}_i(\mathbf{r}_k)H\chi^\eta_j(\mathbf{r}_k) , \tag{8}$$

$$S_{ij}=\sum_\kappa W(\mathbf{r}_k)\chi^{*\eta}_i(\mathbf{r}_k)\chi^\eta_j(\mathbf{r}_k) , \tag{9}$$

where $W(\mathbf{r}_k)$ is a weight function at point $\mathbf{r}_k$.

The sample points set used in our study includes not only a pseudorandom diophantine points set,[25,26] but also a regular spherical-volume mesh. We map the diophantine distribution onto an infinite domain representing the region exterior to atomic spheres of some arbitrary radius, using a Fermi distribution.[26] In order to get good wave-function accuracy in core regions near the nucleus, we use an optimized Gaussian surface mesh in conjunction with a radial Simpson's-rule method in spheres around the nuclei.

After solving secular equation (7) to find coefficients $C^\eta_{ji\sigma}$, and using formula (5), we can get molecular-orbital eigenfunctions $\Psi^\eta_{i\sigma}(\mathbf{r})$. In order to determine the Fermi energy and occupation numbers $f_{i\sigma}(\epsilon)$ for each molecular orbital (MO), Fermi-Dirac statistics were used on these MO eigenstates. The cluster charge density was then constructed by summing over all MO's:

$$\rho_{\sigma,\mathrm{cluster}}(\mathbf{r})=\sum_{i=1}^{N} f_{i\sigma}\,|\,\psi_{i\sigma}(\mathbf{r})\,|^2 . \tag{10}$$

In order to calculate the potential by one-dimensional integrations, this charge density was cast in a multicenter—overlapping-multipolar form,[27]

$$\rho_{\sigma,\mathrm{model}}(\mathbf{r})=\sum_{njlm} d^\sigma_{jlm}(n)\rho_j(r_n)Y_{lm}(\hat{r}_n) , \tag{11}$$

where $\mathbf{r}_n=\mathbf{r}-\mathbf{R}_n$, $\mathbf{R}_n$ are atomic sites, and jlm denotes multipoles centered on various nuclear sites at $\mathbf{r}_n$.

The coefficients $\{d^\sigma_{jlm}\}$ were determined by least-squares fitting to the eigenvector density of Eq. (10) with controled accuracy. The radial density basis set of $\{\rho_j\}$ was constructed from spherical atomic densities calculated from the wave-function variational basis, and from several radial functions for each $l=0$ (or $l\le 1, 2, \ldots$) in the fully symmetric representation of molecular point group. The potential can be calculated from this least-squares self-consistent multipolar (SCM) procedure accurately and efficiently.

The total energy in the spin-polarized case can be written as[13]

$$E_{\rm tot}(\mathbf{r})=\sum_{\sigma}\left[\sum_{i} f_{i\sigma}\epsilon_{i\sigma}-\tfrac{1}{2}\int\frac{\rho_{\sigma}(\mathbf{r})\rho(\mathbf{r}')}{|\mathbf{r}-\mathbf{r}'|}d^3r\,d^3r'-\int\rho_{\sigma}(\mathbf{r})[V_{{\rm xc},\sigma}(\mathbf{r})-E_{{\rm xc},\sigma}(\mathbf{r})]d^3r\right]+\tfrac{1}{2}{\sum_{\mu,\nu}}'\frac{Z_{\mu}Z_{\nu}}{r_{\mu\nu}}\ , \tag{12}$$

where $E_{{\rm xc},\sigma}(\mathbf{r})$ is exchange and correlation energy, $V_{{\rm xc},\sigma}(\mathbf{r})$ is the exchange and correlation contribution to the chemical potential (or so-called exchange potential) with spin direction σ. $E_{{\rm xc},\sigma}(\mathbf{r})=\frac{3}{4}V_{{\rm xc},\sigma}(\mathbf{r})$ for the effective potential of Eq. (4).[22] Total energies of our clusters are on the order of 10^5 eV, and not calculated accurately enough to directly check the energy difference, when we change the position of muon in the copper lattice. The integration errors in Eq. (12) are larger than the accuracy which we need. Fortunately, the main interest we have is not in the large total energy, but rather in more accurate binding energies with respect to some reference system, e.g., the dissociated molecule

$$E_b(\mathbf{r})=\Delta E_{\rm tot}(\mathbf{r})=E_{\rm tot}(\mathbf{r})-E_{\rm tot}^{\rm ref}(\mathbf{r})\ . \tag{13}$$

Binding energies E_b are on the order of a few electron volts per atom. When we calculate the binding energies, the numerical noise still must be kept under control in order to obtain useful results. Systematic errors are estimated to be a few tenths of an electron volt, which is sufficient to determine binding site preference of the muon.

III. RESULTS

A. Muon in Cu_{14} cluster

Copper has the fcc structure with a lattice constant (bulk) of $a_0=3.615$ Å.[28] In these calculations, we treated an isolated cluster including 14 copper atoms and an interstitial muon. In order to study possible binding sites, the muon was put at different positions along the body diagonal. Figures 1 and 2 show the μ-Cu_{14} geometries and coordinate systems for the O_h (μ at center) and C_{3v} cluster symmetries. In these figures, numbers 1 to 13 denote the μ^+ positions, calculated at equal intervals. Positions 1 and 7 are octahedral (O) and tetrahedral (T) sites, respectively. When the muon is put at position 1, the point-group symmetry of the cluster is O_h, and at positions 2—12 the symmetry is C_{3v}. The muon was also slightly displaced from the body diagonal to check muon stability with respect to [111] positions. For example, several positions were chosen displaced from the tetrahedral position 7, along the coordinate axis x direction (see Fig. 2). In that case, the symmetry is only C_{1h}, i.e., there is one mirror plane.

The atomic orbitals used in the molecular-orbital expansion were obtained by solving the self-consistent free-atom problem using the Hartree-Fock-Slater scheme. Spherical wells of varying depth and radial extent were added to the atomic potentials to confine diffuse orbitals. For the muon, as in previous hydrogen impurity studies, basis sets consisting of $1s$, $2s$, and $2p$ orbitals were calculated with a well depth of 2 a.u., with a sloping wall beginning at a radius of 5 a.u. For copper, the same kind of potential well was used: the Cu variational basis set consisted of $4s$, $4p$, and $4d$ orbitals with the $1s,\ldots,3d$ core frozen. The spectroscopic and binding-energy properties of pure Cu_N clusters, $N\leq 79$, were described in Ref. 13; the top of the $3d$ "band" lies ~ 2 eV below the Fermi energy and resembles that found in band-structure calculations. In preliminary studies on μ-Cu_{14} we included the Cu $3d$ orbitals in the variational space, and found them to be completely occupied, as is expected. These orbitals were treated in the frozen-core approximation in all subsequent calculations; they are of course included properly in the binding-energy algorithm. Both $2s$ and $2p$ orbitals in the muon case and both $4p$ and $4d$ orbitals in the copper case were empty orbitals of atoms, included in the basis set in order to ensure variational freedom sufficient to calculate accurate binding energies.

The integration mesh used for this cluster consisted of 300 diophantine points per atom, augmented by regular grids in atomic spheres. Six angular points times 30 radial points were used in the Cu cores, and a more accurate 12×40 mesh was used for the μ region to guarantee an accurate representation of the cluster region critical to binding-energy comparisons.

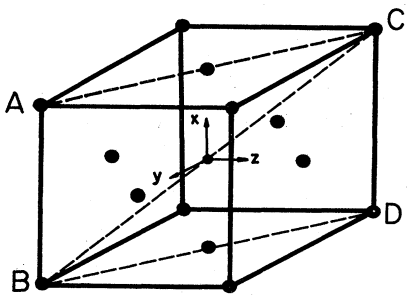

FIG. 1. μ-Cu_{14} (O_h) cluster geometry: An interstitial μ is at the center of fcc Cu_{14}, the octahedral site. The large black circles indicate Cu atoms; the small one indicates the μ. The lattice constant $a_0=3.615$ Å.

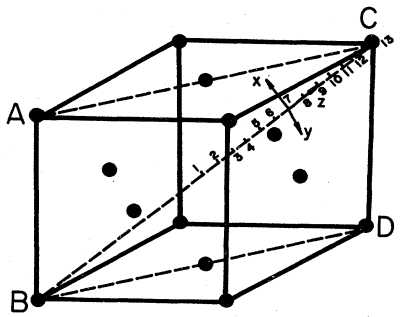

FIG. 2. μ-Cu_{14} (C_{3v}) cluster geometry: An interstitial μ is placed along the body diagonal. Numbers 1—13 denote the μ^+ positions, calculated at equal intervals from the center 1 to the body corner 13. The symmetry for the muon at sites 2—13 is C_{3v}; site 7 is the tetrahedral position. The large black circles indicate Cu atoms; the small black circle indicates the muon. Lattice constant $a_0=3.615$ Å.

For comparison with host properties, calculations were made for the "bare" Cu_{14} cluster with O_h symmetry without the muon present. Figure 3 shows the Coulomb potential V^{e^+} for an unscreened $+1$ test charge in the bare cluster, versus the distance D from the center of the cluster to the field point $\mathbf{r}$ along the [111] line. From this figure, we can see that the Coulomb potential curve displays two minima, corresponding to the O site and the T site. The O-site potential is about 2 eV lower than that of the T site.

In order to find the most stable site for μ^+ in Cu, we should calculate the potential acting on muon, $V^{\mu^+}(\mathbf{r})$ or the total binding energy $E_b(\mathbf{r})$ for the Cu cluster, including an interstitital muon when the muon is at different places. The potential acting on a positive muon depends in turn upon the μ^+ position and its portable screening charge. Our molecular calculation directly gives the potential acting on the muon at position $\mathbf{r}_\mu$, in terms of the electron Coulomb potential $V_C(\mathbf{r})$:

$$V^{\mu^+}(\mathbf{r}_\mu) = -\lim_{r\to r_\mu}\left[V_C(\mathbf{r}) + \frac{1}{|\mathbf{r}-\mathbf{r}_\mu|}\right]. \tag{14}$$

Here $|\mathbf{r}-\mathbf{r}_\mu|$ is the distance between the field point $\mathbf{r}$ and the muon site $\mathbf{r}_\mu$. Equation (14) simply represents the removal of the μ^+ self-interaction and the choice of sign for its positive charge.

The resulting V^{μ^+} potential in μ-Cu_{14} for the muon placed at different sites along the [111] direction is shown in Fig. 4. Calculated points are indicated by dots. For every indicated point, we made a complete molecular SCF-$X\alpha$-DVM calculation. From Fig. 4, the V^{μ^+} curve is seen to have two valleys like the unscreened $+1$ charge Coulomb potential in the pure Cu cluster, corresponding to O and T sites. The V^{μ^+} of O and T sites are -27.65 and -26.40 eV, respectively; the O site thus exhibiting greater binding. Since the zero-point motion of the μ^+ is rather large, it is necessary to consider dynamical effects at least to low order. This has consequences, for example, for the hyperfine field seen by a muon even at low temperature. Zero-point energy ϵ_0 of the muon was estimated as follows: A harmonic approximation was considered near the minimum of the muon potential. Using the formulas (in atomic units)

$$\epsilon_0 = \frac{\omega}{2}, \quad \omega = \left[\frac{\kappa}{m_\mu}\right]^{1/2}, \quad V^\mu(\mathbf{r}) = \tfrac{1}{2}\kappa(\mathbf{r}-\mathbf{r}_0)^2 \tag{15}$$

[where k, ω, and m_μ are force constant, vibration frequency, and mass of muon ($m_\mu = 206.77 m_e$), respectively], the estimated value of the muon zero-point energy at O site is 0.2 eV. The zero-point energy of the T site is even smaller than this. These zero-point energies are considerably less than the difference of the two potential minima (about 1.25 eV), so we conclude that, even considering the muon vibration, the O site is the most stable site. This conclusion is in agreement with interpretation of the experimental results of Chappert *et al.*[2]

Figure 5 shows the *binding-energy* curve for μ-Cu_{14}, when the muon is placed at different sites along the [111] direction. This curve, like the μ^+ potential curve, shows two minima corresponding to O and T sites; O is again found to be the more stable site. The calculated binding energies of the cluster are also listed in Table I, and are seen to amount to more than 3 eV/atom. The binding-energy difference of O and T sites is 1.2 eV, with an es-

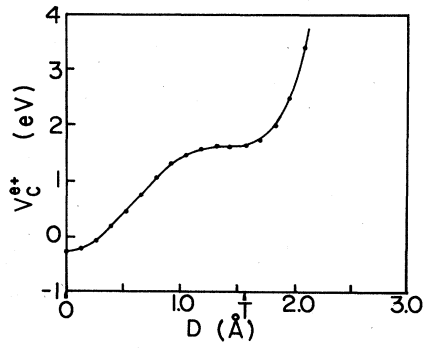

FIG. 3. Unscreened $+1$ charge Coulomb potential V^{e^+} vs the distance D from the center of the cluster Cu_{14} along the [111] direction.

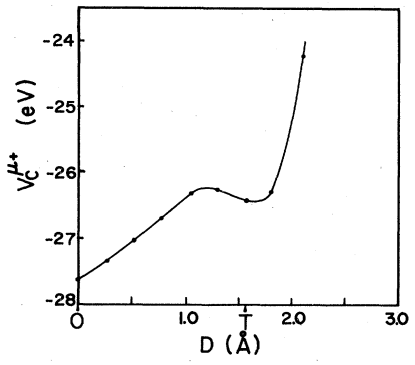

FIG. 4. Coulomb potential seen by the positive muon along [111] in the μ-Cu_{14} cluster scheme. Each dot indicates an individual HFS-$X\alpha$-DVM calculated result. D is the distance from the center of the cluster to the μ site. The O and T indicate octahedral and tetrahedral sites for μ.

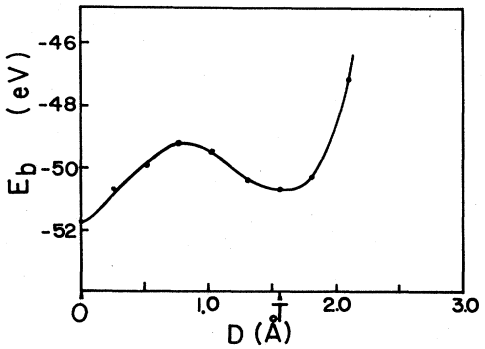

FIG. 5. Binding-energy curve of μ-Cu_{14} for various μ positions along the [111] direction. Each dot indicates an individual HFS-$X\alpha$-DVM calculated results, D is the distance from the center of the cluster to the μ site.

TABLE I. Binding energies of the μ-Cu_{14} cluster for different sites of muon along [111]. D is the distance from the center of the cluster to the muon site. The numbered positions are shown in Fig. 2.

Muon position number	D (Å)	$-E_b$ (eV)
1 (O site)	0.000	51.8
2	0.261	50.7
3	0.522	50.0
4	0.783	49.2
5	1.044	49.4
6	1.304	50.5
7 (T site)	1.565	50.6
8	1.826	50.3
9	2.087	47.1

TABLE II. The electronic charge Q_μ found in the nearest volume surrounding the muon in the μ-Cu_{14} cluster. D is the distance from the center of cluster to the muon site. The position numbers are as shown in Fig. 2.

Muon position number	D (Å)	Q_μ
1	0.000	1.36
2	0.261	1.34
3	0.522	1.37
4	0.783	1.43
5	1.044	1.37
6	1.304	1.32
7	1.565	1.31
8	1.826	1.33
9	2.087	1.30

timated computational uncertainty of ± 0.2 eV. An energy barrier is found between O and T sites, the difference between the top of the barrier and the T site being about 1.4 eV; and the O site is about 2.6 eV. So the O site is more stable than the T site along the [111] direction. The T site is a metastable position for the muon. This conclusion tends to support the model proposed by Seeger[4] for the observed temperature dependence of muon diffusion.

We also calculated binding energies for μ positions near the body-diagonal site. In these low-symmetry clusters, spin polarization was suppressed to simplify the calculation and reduce computer time. Figure 6 shows the binding-energy curve versus muon distance from tetrahedral site 7 along the x-coordinate direction (see Fig. 2). This curve shows the minimum energy to be at the body diagonal (site 7). The spin-restricted binding energy at site 7 in C_{3v} symmetry is -50.84 eV. Comparison with Table I shows that the spin-stabilization energy is ~ 0.24 eV, a reasonable value. Extrapolation of the binding-energy curve of C_{1h} symmetry near site 7 is -50.68 eV. That difference (0.16 eV) provides a measure of calculation error, arising from the low cluster symmetries when the muon is at site 7 (C_{3v}) and off the body diagonal (C_{1h}). The binding curve along the x direction is flatter than along the [111] direction. This means that the muon can move more easily along this direction than along [111], for small displacements. Although computational errors of ~ 0.2 eV are indicated, we can still decide that body-diagonal muon sites are more stable than off-diagonal sites.

Electronic screening of the muon implanted in Cu is of crucial importance for understanding both hyperfine fields and dynamical behavior. The electronic charges $Q_\mu(D)$ found by integration over the nearest volume surrounding the muon placed along [111] are given in Table II. For positions 1—9 the electronic charges range from $1.30e^-$ to $1.43e^-$, indicating that the muon is overscreened. Since the screening is short ranged, the muon can thus move essentially as a neutral particle.

B. A vacancy and an impurity in the μ-Cu system

Because of the recent interest in impurity trapping of the muon,[2] we also calculated the binding energy when a muon interacts with a vacancy or a nickel atom substituting for a cubic-corner Cu atom. This means that in Fig. 2 we use a vacancy or a Ni atom instead of a copper atom at site 13. The clusters considered now become μ-Cu_{13} and μ-Ni-Cu_{13}, with symmetry C_{3v} in both cases.

The binding-energy curve found for the μ-Cu_{13} cluster is given in Fig. 7. Comparing Fig. 7 with Fig. 5, we find large changes due to the vacancy. With a vacancy at site 13, the binding-energy curve also has two valleys; however, the T site is no longer a minimum, and the O site is no

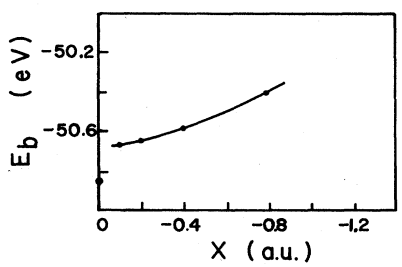

FIG. 6. Binding-energy curve of μ-Cu_{14} with the muon near the body-diagonal site T along the transverse direction $-X$ (see Fig. 2). The dots indicate the individual HFS-$X\alpha$-DVM calculated result. (Spin polarization was not included.)

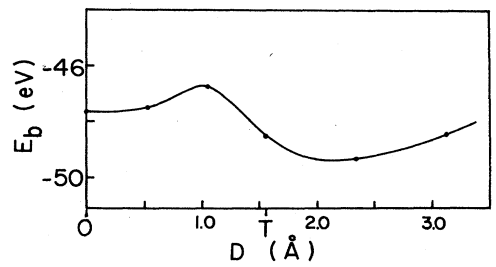

FIG. 7. Binding-energy curve of μ-Cu_{13} (C_{3v}) for various μ positions along the [111] direction. Each circle indicates an individual HFS-$X\alpha$-DVM calculated result. D is the distance from the center of the cluster to the μ.

longer the lowest binding-energy site. The minimum energy is now found between sites 8 and 9 (Fig. 2) at a distance D of about 2 Å from the center of the cluster. The O site is changed to a metastable site, while between O and T there remains an energy barrier. According to this picture, the vacancy will attract the muon, the most stable site being near, but not at, the vacancy site B. We must immediately remark that the small cluster used implies that these results have only semiquantitative value. More quantitative studies could be made in the context of clusters centered on the μ-vacancy "dimer." Our prediction of off-center trapping induced by a vacancy is qualitatively similar to results of a self-consistent jellium calculation on hydrogen impurities in Al and Mg.[29] Interactions with the ionic cores were included in this case by a pseudopotential perturbation scheme.

For treating the impurity Ni case, a nickel atomic basis set was calculated by solving the self-consistent free-atom problem with a spherical well with a depth of 2 a.u. and a sloping wall beginning at a radius of 5 a.u. The variational basis for Ni consisted of $3d$, $4s$, and $4p$ orbitals, with the $1s, \ldots, 3p$ core frozen. The resulting binding-energy curve is shown in Fig. 8. Comparing Fig. 8 with Fig. 5, we can see, with the impurity Ni placed at site 13, the binding-energy curve is essentially shifted towards Ni. Two minima remain but now move to about site 4 ($D \approx 0.75$ Å) and site 9 ($D \approx 2.1$ Å). E_b at site 4 is a little lower than that found for site 9; however, we note that differences in binding energy for these two shallow traps are of the same order as systematic errors in the calculation. Thus, the O and T sites are no longer stable sites for the muon; in fact, they lie near the top of the two barriers of this binding-energy curve. These analyses clearly indicate that Ni impurities also present an attractive potential for the muon.

These conclusions are in agreement with the muon-spin rotation experiment of Chappert *et al.*[2] Their results indicate that μ^+ will become trapped in imperfect regions caused by substitutional impurities, as for example, with Ni in a Cu crystal.

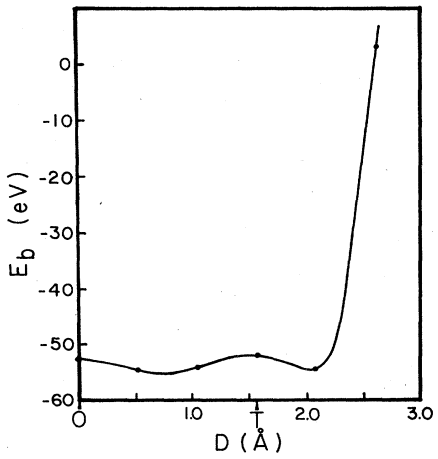

FIG. 8. Binding-energy curve of μ-Ni-Cu_{13} (C_{3v}) for various μ positions along the [111] direction. Each dot indicates an indivual HFS-$X\alpha$-DVM calculated result. D is the distance from the center of the cluster to the muon site.

C. Charge densities

Contour maps of the valence charge densities in the various clusters considered are presented in Figs. 9–11. In all these maps, the planes examined are (110) (i.e., *ABCD* plane in Figs. 1 and 2), and the linear-step contour interval is set at 0.054 $e/$Å^3. In these maps, the valence density mainly includes μ $1s$, Cu $4s$, and Ni $3d,4s$ charge. The virtual state μ $2s,2p$ and metal $4p,4d$ contribute very little to the occupied orbitals.

In Figs. 9(a)–(c), the maps correspond to the muon at

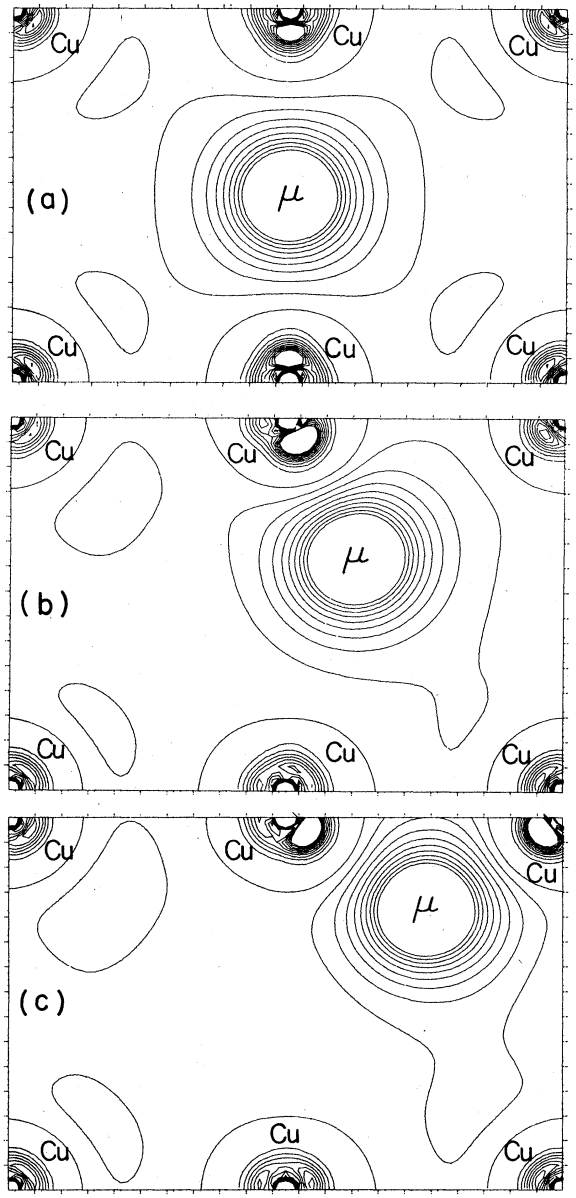

FIG. 9. Valence charge-density maps for the (110) plane (see Fig. 2, *ABCD* plane) in the μ-Cu_{14} cluster. (a) μ at the octahedral site (position 1). (b) μ at position 4. (c) μ at the tetrahedral site (position 7). The linear-step contour interval and the first contour are 0.0540 $e/$Å^3. The unit of distance is in Bohr atomic units.

octahedral (position 1), position 4, and tetrahedral (position 7) sites along the body diagonal, respectively. These maps reveal the bond formed between muon and its Cu near neighbors. The muon environment is seen to be only slightly distorted from spherical shape when the particle is at the octahedral site. But when the muon moves along [111] towards the body corner Cu atom, the environment becomes significantly distorted. When the muon is at position 4, it mainly has one bond connecting with the nearest-neighbor Cu atom, and at position 7, it has two bonds connected to near neighbors. These nonlinear relaxation processes of electronic response to different muon positions have consequences for the potential field V^{μ^+} controlling the muon dynamics. Recently Puska and Nieminen carried out wave mechanical solutions for light impurity distributions in metals, using a potential derived from atomic superposition models.[30] We suggest that the present approach is capable of providing necessary improvements to their effective-medium approach, which would make the dynamics completely self-consistent.

The corresponding Cu-vacancy case is shown in Fig. 10. The near muon environment is also only slightly distorted from spherical shape, when the muon is at the O site, and weakly bonded to neighboring atoms. The relax-

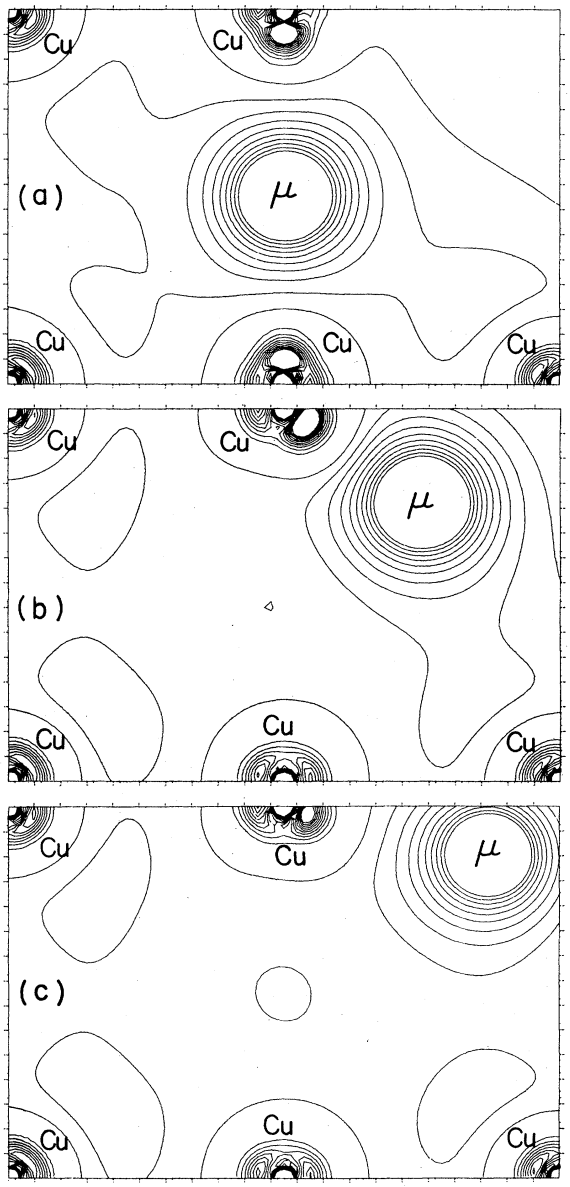

FIG. 10. Valence charge-density maps for the (110) plane (see Fig. 2, *ABCD* plane) in μ-Cu_{13}. (a) μ at the octahedral site (position 1). (b) μ at the tetrahedral site (position 7). (c) μ at position 10. The linear-step contour interval and the first contour is 0.0540 $e/\text{Å}^3$. The unit of distance is in atomic units.

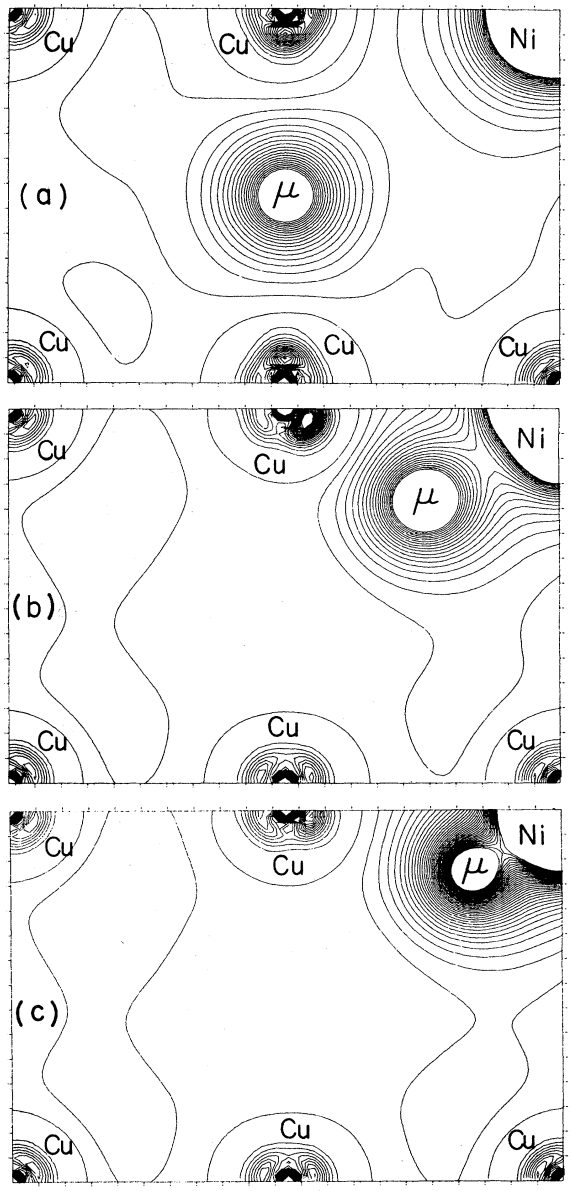

FIG. 11. Valence charge density maps for the (110) plane (see Fig. 2, *ABCD* plane) in μ-Ni-Cu_{13}. (a) μ at the octahedral site (position 1). (b) μ at the tetrahedral site (position 7). (c) μ at position 9. The linear-step contour interval and the first contour is 0.0540 $e/\text{Å}^3$. The unit of distance is in atomic units.

ation of the screened muon into its minimum energy configuration can be visualized by comparing Fig. 10(b) (site 7) with 10(c) (site 10).

Valence charge maps are shown in Fig. 11, for the μ-Ni impurity cluster. These maps show the muon at different sites along the [111] direction. When the muon is at the O site, two bonds of the muon connect with two near copper neighbors, and a polarization toward the distant Ni is already visible. When the muon moves to tetrahedral site 7 and site 9, the main bonding of the muon develops toward the substitutional Ni impurity. Figure 11(c) shows the stablest position for muon in the μ-Ni-Cu_{13} cluster, where a dimer μ-Ni clearly has formed. Because the atomic numbers of Ni and Cu are 28 and 29, respectively, it is easy to understand how, from the viewpoint of a conduction electron, the μ^+-Ni dimer can minimize the energy of the system by essentially restoring the crystal "ionic cores" to their unperturbed state. Such qualitative arguments are, of course, most useful after the fact of detailed energy calculations.

IV. SUMMARY

The electronic structure and associated properties of light impurities in metals is an interesting problem, with extensive implications for applications. Experimentally, the muon-spin-rotation (μSR) technique has given a large amount of data on the muon motional behavior, which has to be correlated with microscopic-theoretical predictions. We thus require detailed knowledge of the electronic structure, potential energy, and binding energy of muons in the host lattice. In this paper, the Hartree-Fock-Slater one-electron local-density theory has been used to calculate binding-energy and potential-energy curves for muons in small Cu clusters, and in clusters containing either a vacancy or a Ni impurity.

In treating clusters with an interstitial muon differment positions of the μ^+ along the body diagonal [111], and slightly displaced from the diagonal, covering the path including octahedral and tetrahedral sites were considered. When the muon is translated along the body-diagonal direction, both binding energy $\Delta E_{\text{tot}}(\mathbf{r})$ and muon potential $V^{\mu^+}(\mathbf{r})$ exhibit a double minimum at O and T sites. The O site is more stable (in the low-temperature, frozen lattice limit treated here); the T site is metastable. When slightly displaced from the body diagonal, the μ^+ binding energy decreases, suggesting that the body-diagonal line does indeed represent a minimum energy configuration for the system. The preceding conclusions are in good agreement with interpretations of the μSR experiments.[2]

The cases of Cu vacancy or Ni impurity were also investigated. In the Cu-vacancy case, the binding-energy curve along [111] still has two minima, but the more stable site is no longer O, changing to a position between T and the vacancy site. In the Ni case, the binding-energy curve again shows two minima, this time shifted toward the impurity Ni and forming a μ^+-Ni dimer. This means that vacancy and impurity Ni both attract muons in accordance with previous interpretations. We have quantitatively determined the binding energy and equilibrium geometry in each case.

From the contour maps of the valence charge densities in μ-Cu_{14}, μ-vacancy-Cu_{13}, and μ-Ni-Cu_{13} clusters, the muon environment is seen to be only slightly distorted from spherical shape when the μ^+ is far from a metal atom. The electronic screening length is seen to be quite short, and a nearest volume integration indicates overscreening. When the muon is moved along the [111] direction, the bonding of the muon to near neighbors becomes evident. In the Ni-impurity case, the formation of a strong μ-Ni bond for the stablest position is quite apparent. It is suggested that a combination of a self-consistent electron response, as calculated here, with lattice-relaxation muon distribution models, as given in Ref. 30, can lead to quantitative understanding of self-trapping and diffusion.

ACKNOWLEDGMENTS

This work was supported by NSF Grant No. DMR82-14966. We thank B. Lindgren and E. Karlsson for helpful discussions. Calculations were carried out in part in the Minicomputer Facility of the Northwestern University Materials Research Center, supported in part under the NSF-MRL program, Grant No. DMR82-16972.

*Permanent address: Department of Physics, University of Science and Technology of China, Hefei, Anhui, The People's Republic of China.

[1]J. H. Brewer, K. M. Crowe, F. N. Gygax, and A. Schenck, in *Muon Physics,* edited by V. W. Hughes and C. S. Wu (Academic, New York, 1975), Vol. II.

[2]J. Chappert, A. Yaouanc, O. Hartmann, E. Karlsson, L.-O. Norlin, and T. O. Niinikoski, Solid State Commun. **44**, 13 (1982).

[3]C. W. Clawson, K. M. Crow, S. S. Rosenblum, and S. E. Kohn, Phys. Lett. **51**, 114 (1983).

[4]A. Seeger, Phys. Lett. **93A**, 33 (1982); A. Seeger, Appl. Phys. **7**, 85 (1975).

[5]A. M. Stoneham, Hyperfine Interact. **17-19**, 53 (1984); S. Estreicher and P. F. Meier, *ibid.* **17-19**, 241 (1984); M. Doyama, N. Nakai, and R. Yamamoto, *ibid.* **17-19**, 231 (1984); S. Tanigawa, K. Ito, Y. Iwase, S. Terakado, K. Nagamine, N. Nishiyama, and T. Suzuki, *ibid.* **17-19**, 235 (1984).

[6]V. G. Grebinnik, K. Nagamine, N. Nishiyama, and T. Suzuki, J. Exp. Theor. Phys. **68**, 1548 (1976); V. G. Grebinnik *et al.*, Zh. Eksp. Teor. Fiz. **68**, 1548 (1975) [Sov. Phys.—JETP **41**, 777 (1976)].

[7]O. Hartmann, E. Karlsson, L.-O. Norlin, T. O. Niinikoski, K. W. Kehr, D. Richter, J.-M. Welter, A. Yaouance, and J. Le Hericy, Phys. Rev. Lett. **44**, 337 (1980).

[8]H. Schilling, M. Camani, F. N. Gygax, W. Ruegg, and A. Schenck, Hyperfine Interact. **8**, 675 (1981).

[9]O. Hartmann, L. O. Norlin, A. Yaouanc, J. Le Hericy, E. Karlsson, and T. O. Niinikoski, Hyperfine Interact. **8**, 533 (1981).

[10]O. Hartmann, Phys. Rev. Lett. **39**, 832 (1977).
[11]M. Camani, F. N. Gygax, W. Ruegg, A. Schench, and H. Schilling, Phys. Rev. Lett. **39**, 836 (1977).
[12]R. M. Nieminen, Hyperfine Interact. **8**, 437 (1981).
[13]B. Delley, D. E. Ellis, and A. J. Freeman, Phys. Rev. B **27**, 2132 (1983).
[14]B. Lindgren and D. E. Ellis, Phys. Rev. B **26**, 636 (1982).
[15]J. C. Slater, Phys. Rev. **81**, 385 (1951).
[16]J. C. Slater, Phys. Rev. **91**, 528 (1953).
[17]J. C. Slater and K. H. Johnson, Phys. Rev. B **5**, 844 (1972).
[18]J. C. Slater and J. H. Wood, Int. J. Quantum Chem. **4S**, 3 (1971).
[19]E. J. Baerends, D. E. Ellis, and P. Ros, Chem. Phys. **2**, 41 (1973).
[20]E. J. Baerends and P. Ros, Chem. Phys. **2**, 52 (1973).
[21]J. C. Slater, *The Self-consistent Field for Molecules and Solids* (McGraw-Hill, New York, 1974).
[22]W. Kohn and L. J. Sham, Phys. Rev. **140**, A1133 (1965).
[23]D. E. Ellis and G. S. Painter, Phys. Rev. B **2**, 2887 (1970).
[24]T. Parameswaran and D. E. Ellis, J. Chem. Phys. **58**, 2088 (1973).
[25]C. B. Haselgrove, Math. Comput. **15**, 323 (1961).
[26]D. E. Ellis, Int. J. Quantum Chem. **2S**, 35 (1968).
[27]B. Delley and D. E. Ellis, J. Chem. Phys. **76**, 1949 (1982).
[28]*Handbook of Chemistry and Physics,* 63rd ed. (Chemical Rubber Co., Cleveland, Ohio, 1962).
[29]D. S. Larsen and J. K. Norskøv, J. Phys. F **9**, 1975 (1979).
[30]M. J. Puska and R. M. Nieminen, Phys. Rev. B **29**, 5382 (1984).